



Efficient modeling of mistuned blade aeroelasticity using fully-coupled two-scale method

H.M. Phan^{a,b,*}, L. He^a

^a Department of Engineering Science, University of Oxford, Oxford OX2 0ES, United Kingdom

^b Department of Mechanical Engineering Sciences, University of Surrey, Guildford GU2 7XH, United Kingdom

ARTICLE INFO

Article history:

Received 2 July 2021

Received in revised form 3 October 2022

Accepted 6 October 2022

Available online 31 October 2022

Keywords:

Turbomachinery

Forced response

Aeroelasticity

Fluid–structure interaction

Mistuning

ABSTRACT

Blade-to-blade variations, known as mistuning, significantly affect the turbomachinery aeroelastic performance. Typically mistuning is observed to be beneficial for flutter stability but detrimental for forced response. In some unconventional cases however, mistuning may even result in a benefit in forced response as reported by some researchers. Many previous studies indicated that neglecting the mistuning-induced changes in aerodynamic forcing and damping would lead to erroneous results. To include these aerodynamic effects, the natural approach is to perform a fully-coupled multi-passage simulation. However, it is apparent that this approach would need a higher simulation cost. In this paper we propose an efficient two-scale method for fully-coupled simulations. The validity and effectiveness of the method is demonstrated in forced response case studies for a mistuned bladerow. The proposed methodology is shown to be by one order of magnitude faster than the baseline fine-mesh simulations, while having a similar accuracy.

© 2022 The Author(s). Published by Elsevier Ltd. This is an open access article under the CC BY-NC-ND license (<http://creativecommons.org/licenses/by-nc-nd/4.0/>).

1. Introduction

The efficiency and reliability of gas turbines have always been primary interests of both the aviation and power generation industries. One of the main challenges in gas turbine development is the aeromechanical vibration due to the interaction between the blades and the surrounding flow. This can give rise to the flutter and forced response problems. The former is self-excited, while the latter undergoes an excessively high number of vibration cycles under the effect of fluid disturbances (i.e. wakes, potential fields, etc.). These vibration cycles induce additional dynamic stresses on the blades, undermining their structural integrity and leading to pre-matured failures. Thus, it is essential to predict accurately the vibration amplitude under the resonance condition. The forced response problem will therefore be a case study of interest in the present work.

As of today, it is the industry standard to predict the forced response amplitude using the uncoupled methods (Chiang and Kielb, 1993; Moffatt et al., 2005). For the conventional turbomachinery blades with high mass ratio, the fluid–structure interaction effects are assumed to be small and the use of uncoupled methods is justified (Sadeghi and Liu, 2005; Moffatt and He, 2005; Chahine et al., 2019). The uncoupled forced response prediction process starts with the identification of the dangerous resonance crossings using the Campbell Diagram. The blade eigen-frequency, modeshape, rotational speed, and engine order of the vulnerable operating conditions can be determined. The separate uncoupled simulations with imposed modeshape, frequency, and nodal diameter of interest are carried out to obtain the modal aero-forcing and aero-damping.

* Corresponding author at: Department of Engineering Science, University of Oxford, Oxford OX2 0ES, United Kingdom.
E-mail address: h.phan@surrey.ac.uk (H.M. Phan).

Nomenclature

GISM	Generalized influence superposition method
IBPA	Inter-blade phase angle
ICM	Influence coefficient method
UST	Unsteady source term
C	Blade chord
C_{ax}	Blade chord projected to the axial direction
C_p	Steady pressure coefficient; $C_p = (p - p_2) / (p_{01} - p_2)$
C_{p1}	First harmonic unsteady pressure coefficient
ω	Angular frequency
k	Reduced frequency; $k = \omega C / V_{ref}$
m	Blade number index
N	Total number of blades in full-wheel assembly
N_d	Number of disturbances
N_f	Number of Fourier harmonics
N_θ	Number circumferential Fourier harmonics
P_{01}	Inlet total pressure
P_2	Outlet static pressure
S	Blade pitch
V_{ref}	Reference isentropic exit velocity; $V_{ref} = \sqrt{2(p_{01} - p_2) / \rho}$
x	Axial chordwise distance
σ	Interblade phase angle, IBPA
γ	Stagger angle

These aerodynamic-induced parameters are then fed to the structure solver to find the harmonic amplitude response. If the blades are assumed to be tuned, there are existing methods to calculate the aero-forcing and aero-damping in an efficient way. These methods are based on the single-passage phase-shifted method, which represents the state-of-the-art in aeroelasticity modeling (He, 2010). The aero-forcing due to the adjacent bladerows' effects can be predicted efficiently using the methods, e.g. in Refs. Giles (1990), Chen et al. (2001), Hall and Ekici (2005) and Sicot et al. (2012). On the other hand, the aero-damping of the oscillating bladerow is calculated using the methods, e.g. in Refs. He and Ning (1998), Hall et al. (2002) and Sicot et al. (2014).

However, there are inevitably blade-to-blade variations due to manufacturing and assembly processes as well as wear and tear during operation. The inherently stochastic variations, known as mistuning, break the tuned idealization assumption. This leads to a considerable change in aero-forcing and aero-damping from the fluid side. Phan and He (2021) showed that random mis-staggering within a small range of ± 1 deg can induce up to $\pm 20\%$ change in the time-averaged loading, while the dynamic loading was also observed to vary significantly. More remarkably, the present authors have demonstrated in the recent work the capability to improve the blade aeroelastic performance by designing a phasing between the structural mistuning pattern and the aerodynamic mistuning pattern (Phan and He, 2022a). Leng and Key (2020) reported that a sinusoidal spacing pattern can induce an unsteady loading three times higher than the tuned blade. Nevertheless, these aerodynamic variations have been observed to be important in predicting an accurate response of the mistuned blades. He et al. (2007) found that the aerodynamic coupling significantly affects the bladed disk vibrations. They proposed a reduced-order approach to calculate the unsteady aerodynamic forces directly using the tuned system modes. Miyakozawa et al. (2009) showed that the aerodynamic asymmetric perturbations can increase significantly the maximum blade amplitudes. The effects of aerodynamic asymmetry are calculated by perturbing the influence coefficient matrix. However, only the aero-asymmetry due to blade motion was taken into account while that due to forcing was not. Petrov (2010) proved that the inclusion of aerodynamic damping and coupling was important for an accurate prediction of forced response levels. He proposed a method based on the Frequency Response Function matrix to include the aerodynamic effects in the forced response calculation. The method was applied to a bladed disk, which revealed a new phenomenon of the forced response level reduction by mistuning. Martel and Sánchez-Álvarez (2017) applied the Asymptotic Mistuning Model and found that the mistuned damping variation can also result in a reduction of the forced response level.

With the background introduced so far, one can see that mistuning variations can significantly affect the forced response levels. In addition, the aeroelastic coupling between the blades and the surrounding fluid will also play a crucial role as a lighter material becomes possible. On the other hand, the variations of aero-forcing and aero-damping are difficult to be modeled efficiently due to the stochastic nature of mistuning, particularly if using the common single-passage phase-shifted model. A more natural way of including the aerodynamic effects of mistuned variations is by performing the fully-coupled multi-passage simulations. However, the fully-coupled method is already expensive on its own. This

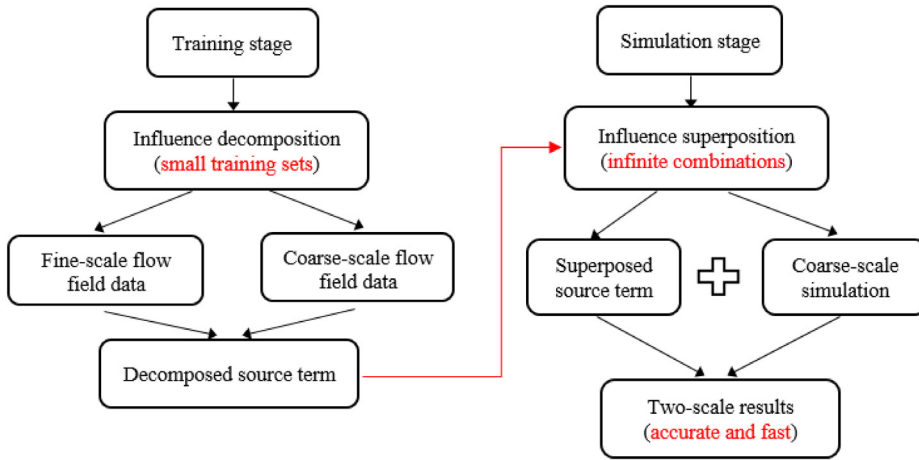


Fig. 1. Overview of the two-scale method combined with the Generalized Influence Superposition approach.

problem is exacerbated by the inclusion of multi-passage domains accommodating a stochastic mistuning distribution. There have been some data-driven approaches for aeroelastic problems (Tran, 2009; Su et al., 2016; Kelly et al., 2021). Although they are efficient, they rely on a sufficiently large database. Its accuracy in extrapolation cases can be erroneous and is still a subject of development.

In the present work, we introduce a fully-coupled approach combined with the two-scale method to investigate the mistuned forced response problems more efficiently while having an accuracy comparable to that of the direct fully-coupled fluid–structure solutions. The newly proposed method can fulfill the two seemingly conflicting criteria of simulation cost and accuracy thanks to the use of the two-scale approach. The use of coarse mesh in the two-scale simulation reduces the simulation time. However, there is no loss of accuracy due to the coarse mesh because of the source term's correction effect. Another aspect of modeling interest is the use of the Generalized Influence Superposition method (GISM) to reconstruct the source term variations due to mistuning from the set of tuned samples. In the following sections, we will present the methodology first. Then we will validate the new method against the direct fully-coupled fluid–structure interaction solutions for the tuned, alternately mistuned, and randomly mistuned bladerows.

2. Numerical methods

2.1. Method overview

The present method consists of the training stage and the simulation stage. In the training stage, the method starts with pre-requisite flow fields of a finite-passage tuned influence cascade computed using both fine-scale and coarse-scale models for the same configurations. The fine-scale flow field is then projected onto the coarse-scale representation with a reduced mesh resolution. Sets of source terms will be created as a result to recover the fine-scale flow field based on the low-scale simulation. The source terms will be decomposed into influence terms.

In the simulation stage, the required source terms can be predicted and superimposed using the Generalized Influence Superposition method (details of this method will also be presented in the next section). The coarse-scale simulations are run altogether with the estimated source terms, which improves the accuracy (thanks to the source terms) and reduces the simulation time (thanks to the coarse-scale representation). More remarkably, the influence terms obtained from the tuned cascade can be used to approximate an infinite combinations of mistuning patterns, which further increases the method's efficiency. It will also be shown that the interaction among blades in the cascade can also be captured in the two-scale simulations. Fig. 1 illustrates the overview of the two-scale method combined with the Generalized Influence Superposition approach.

2.2. Governing equations

The fully-coupled fluid–structure interaction method adopted in the present work follows the partitioned scheme. In the partitioned scheme, the fluid and structure governing equations are solved separately by their dedicated solvers. An outer time step loop represents the time-marching with a physical time step, which contains several inner loops. Data between two solvers are exchanged after each inner time step loop, thus representing a tightly-coupled system.

On the fluid side, the unsteady Navier–Stokes equations are solved for:

$$\frac{\partial \rho}{\partial t} + \nabla \cdot (\rho \mathbf{U}) = 0$$

$$\begin{aligned} \frac{\partial (\rho \mathbf{U})}{\partial t} + \nabla \cdot (\rho \mathbf{U} \otimes \mathbf{U}) &= -\nabla p + \nabla \cdot \boldsymbol{\tau} \\ \frac{\partial (\rho H)}{\partial t} - \frac{\partial p}{\partial t} + \nabla \cdot (\rho \mathbf{U} H) &= \nabla \cdot (\lambda \nabla T) + \nabla \cdot (\mathbf{U} \cdot \boldsymbol{\tau}) \end{aligned} \quad (1)$$

The governing equations represent the conservation of mass, momentum, and energy at each instantaneous time level. To close the equations, the $\gamma - \theta$ transition correlation coupled with the Shear Stress Transport (SST) model is adopted. On the solid side, the rigid body equations of motion are solved separately for bending and torsion vibration modes:

$$\begin{aligned} \frac{dP}{dt} &= F_{aero} - k_{bending} (x - x_{COM}) \\ \frac{d\Gamma}{dt} &= M_{aero} - k_{torsion} (\theta - \theta_{COM}) \end{aligned} \quad (2)$$

where P is linear momentum, Γ is angular momentum. F_{aero} and M_{aero} denote the aerodynamic force and moment acting on the blade, respectively. Similarly, $k_{bending}$ and $k_{torsion}$ represent the stiffness in the respective degree of freedom.

3. Generalized influence superposition method

Based on the linear superposition principle, the total effects acting on a reference blade embedded within an oscillating bladerow can be expressed as the summation of the effects of each blade of the bladerow vibrating individually respectively. In the most general form, the linear superposition can be expressed as:

$$U_{total}(t) = \sum_{m=-N/2}^{+N/2} U_m(t) \quad (3)$$

where U_{total} is the total effects acting on a reference blade in an oscillating bladerow; U_m is the individual effect originated from the vibrating blade m while all other blades are kept stationary. The index m is counted from the reference blade ($m = 0$). Thus U_0 is the influence of the vibrating blade on itself. N is the total number of blades in the whole annulus assembly.

Eq. (3) is intentionally expressed in the time domain as we are interested in a more general mistuned situation where neither should a constant frequency, nor a constant interblade phase angle for a vibrating bladerow be assumed. Using a Fourier decomposition approach, the time series data is converted to a frequency domain representation with infinite number of harmonics:

$$U_{total}(t) = \sum_{m=-N/2}^{+N/2} \sum_{n=1}^{\infty} A_{m,n} \sin(n\omega_m t + \theta_{m,n}) \quad (4)$$

where $A_{m,n}$ and $\theta_{m,n}$ is the amplitude and phase originated from the blade m with n th harmonics, respectively; ω_m is the fundamental vibration frequency of blade m .

The Fourier series in Eq. (4) can be approximated by including up to N_f harmonics:

$$U_{total}(t) \approx \sum_{m=-N/2}^{+N/2} \sum_{n=1}^{N_f} A_{m,n} \sin(n\omega_m t + \theta_{m,n}) \quad (5)$$

For some cases such as oscillating blades, each blade would typically have a dominant and well-characterized fundamental frequency. Thus, it can be reduced further to include only the term with fundamental frequencies ω_m :

$$U_{total}(t) \approx \sum_{m=-N/2}^{+N/2} A_{m,1} \sin(\omega_m t + \theta_{m,1}) \quad (6)$$

where $A_{m,1}$ and $\theta_{m,1}$ is the 1st harmonic amplitude and phase originated from the blade m .

It can be seen from Eq. (6) that each blade m would still have its own vibration characteristics including the fundamental frequency ω_m , the 1st harmonic amplitude $A_{m,1}$, and the 1st harmonic phase angle $\theta_{m,1}$. In the simplest case where all blades are tuned such that each blade would have the same fundamental frequency $\omega_m = \omega = \text{constant}$ and the same interblade phase angle $\sigma = \theta_{m+1} - \theta_m = \theta_m - \theta_{m-1} = \text{constant}$. Applying Eq. (6) to the tuned cascade gives:

$$U_{tuned}(t) \approx \sum_{m=-N/2}^{+N/2} A_{m,1} \sin(\omega t + \theta_{m,1} + m\sigma) \quad (7)$$

where $A_{m,1}$ is the 1st harmonic amplitude of the influence due to the vibrating reference blade on the blade m ; $\theta_{m,1}$ is the 1st harmonic phase of the influence due to the vibrating reference blade on the blade m ; σ is the constant interblade phase angle. The local influence on blade m needs to be shifted back to the reference blade (Blade 0), thus we need the $m\sigma$ term.

Eq. (7) can be written in the complex form, which is exactly the same as in the classical influence coefficient method (e.g. Ref. Hanamura et al. (1980)):

$$U_{tuned}(t) \approx \sum_{m=-N/2}^{+N/2} U_m e^{-im\sigma} \quad (8)$$

where U_m is the local influence on the blade m .

In summary, the Generalized Influence Superposition method described in this section does not need any assumptions regarding the constant frequency, amplitude, and/or phase angle of the oscillating blades. In addition, it has been shown that the Generalized Influence Superposition method is equivalent to the classical Influence Coefficient Method if the tuned cascade assumptions apply.

4. Two-scale approach

4.1. Basis of two-scale approach

The two-scale method is a source term-based approach. It was originally developed to solve problems with disparate length and time scales (He, 2013, 2018). It has typically found the applications where many repetitive small-scale elements are present such as cooling holes and additively manufactured micro-patterns. Recently, it has been extended and developed for the first time within the commercial solver framework to deal with the unsteady flow and the grid deformation, which coincides with the requirement of aeroelasticity applications (Phan and He, 2021). In this section, the basis of the two-scale method is presented for clarity as we will gradually introduce its coupling with the fully-coupled fluid-structure interaction method.

The unsteady Navier–Stokes equations can be written in a semi-discrete form:

$$\frac{\partial}{\partial t}(\mathbf{U}) + R(\mathbf{U}) = 0 \quad (9)$$

The conservative flow variable \mathbf{U} is a seven-element vector for a three-dimensional unsteady flow with two-equation turbulence model, $\mathbf{U} = [\rho \ \rho u \ \rho v \ \rho w \ \rho E \ \rho k \ \rho \omega]^T$. $R(\mathbf{U})$ is the lumped advection and diffusion terms.

If the domain is discretized using a fine mesh resolution Ω_f , the instantaneous governing equations have to be satisfied once the simulation converges:

$$\frac{\partial}{\partial t}(\mathbf{U}_f) + R_f(\mathbf{U}_f) = 0 \quad (10)$$

Supposing the same flow domain is now discretized with a coarse mesh resolution Ω_c . The poorly resolved but converged coarse mesh solution still satisfies the equations:

$$\frac{\partial}{\partial t}(\mathbf{U}_c) + R_c(\mathbf{U}_c) = 0 \quad (11)$$

To recover the accurate fine mesh solution on the base coarse mesh domain, the two-scale computation aims to solve for the fine-to-coarse interpolated solution. The projection from fine to coarse mesh discretization is through the volume-weighted averaging process:

$$\mathbf{U}_{f \rightarrow c} = \frac{1}{\Delta V_c} \sum \mathbf{U}_f \Delta V_f \quad (12)$$

where the summation is taken for all the fine mesh cells of volume ΔV_f corresponding to a coarse mesh cell of ΔV_c .

The volume-weighted averaging solution $\mathbf{U}_{f \rightarrow c}$ to be recovered in the two-scale simulation must also satisfy the governing equations (Eq. (9)). However, due to the difference between the projected solution $\mathbf{U}_{f \rightarrow c}$ and the coarse mesh solution \mathbf{U}_c , the projected solution $\mathbf{U}_{f \rightarrow c}$ does not satisfy the governing equations on the base coarse mesh discretization:

$$\frac{\partial}{\partial t}(\mathbf{U}_{f \rightarrow c}) + R_c(\mathbf{U}_{f \rightarrow c}) \neq 0 \quad (13)$$

Eq. (13) can then only be balanced if a source term is introduced to the right-hand side of the equations (Phan and He, 2021; Ning and He, 2001):

$$\frac{\partial}{\partial t}(\mathbf{U}_{f \rightarrow c}) + R_c(\mathbf{U}_{f \rightarrow c}) = \mathbf{UST} \quad (14)$$

where \mathbf{UST} is the unsteady source term arisen due to the spatial resolution reduction. It is also a seven-element vector, where each entry is to balance its corresponding governing equations at anywhere in space and time.

Now it is clear that the basic idea of the two-scale approach is to introduce an appropriate spatial–temporal source term to recover the projected fine mesh solution on the coarse mesh discretization of the two-scale computation. However, the introduction of the unsteady source term **UST** leads to a closure problem. In the authors' previous work for uncoupled simulations (Phan and He, 2021), we have proposed for the first time that the source term can be split into a time-averaged component and a time-varying component. In addition, the time-varying components can be further split into different contributing factors to include effects due to multiple disturbances. In Ref. Phan and He (2021), we have also demonstrated the need of those source terms in a series of verification and validation test cases. Then each individual constituent source term can be decoupled and pre-computed, which enables the required total source term to be estimated in an efficient manner:

$$\mathbf{UST}_{total} = \overline{\mathbf{UST}} + \sum_{i=1}^{N_d} \mathbf{UST}_i \quad (15)$$

where $\overline{\mathbf{UST}}$ is the steady/time-averaged source term. \mathbf{UST}_i is the time-varying source term due to each disturbance i . N_d is the number of disturbances that the flow field is subject to.

For the forced response problems, the disturbances include the external forcing (e.g. inlet distortion) and the blade vibrations as a response to the forcing. The former is denoted as the *vibration-independent* disturbance, while the latter is denoted as the *vibration-dependent* disturbance. One of the feature of the present work is to split these two disturbances into two independent sources, enabling a more efficient way to estimate the required source term. Each of these sources would also be integrated in the fully-coupled fluid–structure interaction workflow in a different manner.

5. Fully-coupled two-scale approach combining with the generalized influence superposition method

5.1. Fully-coupled two-scale method workflow

The practical integration of the two-scale method in the fully-coupled workflow is presented in Fig. 2. Compared to the original workflow of the partitioned fluid–structure approach, the two-scale method introduces the source terms to the fluid solver (highlighted in red). It can be noted that the vibration-independent and vibration-dependent source term are implemented at different stages of the workflow. The steady/time-average and the vibration-independent source term are implemented within the inner loop iteration. On the other hand, the vibration-dependent source term is implemented at the outer loop level. The underlying reason of this procedure is that the vibration-dependent source term will be updated based on the blade vibration characteristics (e.g. vibration frequency, amplitude, phase angle) after each physical time step. Typically this involves an embedded Fast Fourier Transform (FFT) operation after the outer loop iteration. Once the blade vibration characteristics are identified, the vibration-dependent source term can be scaled accordingly. The calculation procedures of vibration-independent and vibration-dependent source term will be presented in the next section.

5.2. Vibration-independent source term calculation

In the present work, the external forcing originates from the prescribed rotating inlet distortion with the a-priori known forcing amplitude and frequency. Because the source term decomposition is proposed to be pre-computed in a decoupled manner, the bladerow is considered tuned (no blade-to-blade variations) and stationary. A multi-passage direct simulation subject to the inlet distortion needs to be carried out to sample the source term arisen due to the inlet distortion. The spatial Fourier transform method can be used to convert the source term to its frequency-domain representation for optimum storage. Performing discrete Fourier transform at any instantaneous time level, the inlet distortion-originated source term can be calculated using the available circumferential positions:

$$\mathbf{UST}_{distortion} = \sum_{n=1}^{N_\theta} (\mathbf{A}_{U,\theta} \cos(n\theta_m) + \mathbf{B}_{U,\theta} \sin(n\theta_m)) \quad (16)$$

where $\theta_m = 2\pi(m-1)/N$. Note that N_θ is the number of retained spatial harmonics and $2N_\theta + 1 \leq N$.

5.3. Vibration-dependent source term calculation using the generalized influence superposition method

The blades would vibrate as the response to the external forcing. The vibration kinematics including amplitude, frequency, and phase angle are unknown a-priori, particularly in the mistuning context. In the proposed source term decomposition technique, the oscillating bladerow is subject to a uniform inlet condition. The vibration-dependent source term is further decomposed into contributions from different blades as shown in Eq. (17):

$$\mathbf{UST}_{vibration} = \sum_{m=-N/2}^{+N/2} \mathbf{UST}_{vibration,m} \quad (17)$$

where m is the blade number index. N is the total number of blades in the multi-passage assembly.

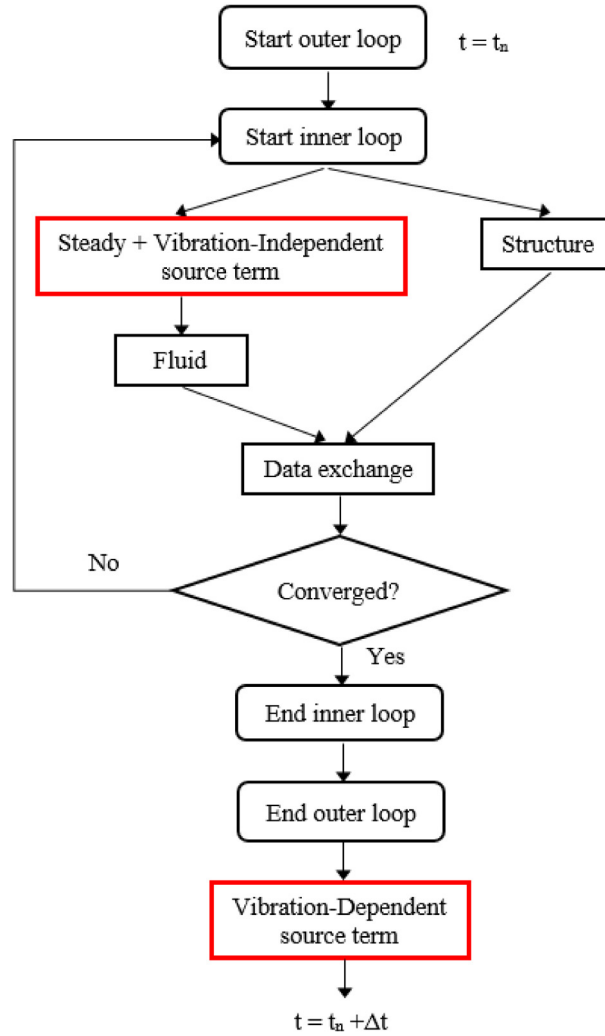


Fig. 2. Illustration of the source term influence coefficient calculation method. (For interpretation of the references to color in this figure legend, the reader is referred to the web version of this article.)

The superposition technique does not need to be confined to the tuned oscillating bladerow problem as typically used in the classical Influence Coefficient Method. We will employ the Generalized Influence Superimposition method (GISM) discussed in the previous section to deal with the mistuning problem. In the GISM method, the mistuned blade response in a full-annulus simulation can be reconstructed based on the superimposed influence of the reference blade itself and its neighbors. The influence can be sampled in a truncated-domain simulation because the effects of further blades diminish. The influence is sampled in the time domain without any assumption on the constant amplitude, frequency and inter-blade phase angle. The GISM method is particularly designed to remove the restriction of tuned bladerow assumptions adopted in the classical ICM. The modification makes the GISM method more superior and suitable for mistuning study compared to the original ICM technique. For optimum storage and practical use, the vibration-dependent source term of the blade m can be converted from the time domain to the frequency domain:

$$UST_{vibration} = \sum_{m=-N/2}^{+N/2} \sum_{n=1}^{N_f} \mathbf{A}m_{m,n} \sin(n\omega_m t + \theta_{m,n}) \quad (18)$$

where m is the blade number index and n is the harmonic index. N_f is the number of retained temporal harmonics. $\mathbf{A}m_{m,n}$, ω_m , and $\theta_{m,n}$ are the amplitude, frequency, and phase angle of the vibration-dependent source term, respectively.

It is clear from Eq. (18) that the blade m would have the corresponding effects on the amplitude, frequency, and phase angle representation of the source term. Those variables are not assumed constant across the bladerow in contrast to the typical ICM's requirement. For practical implementation, the direct simulation of a GISM truncated-domain needs to be

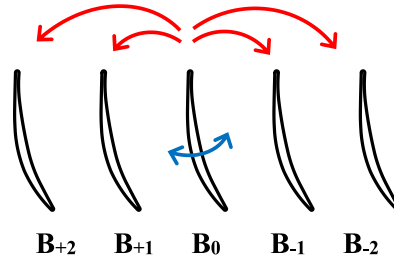


Fig. 3. Illustration of the source term decomposition method for the vibration-dependent source term.

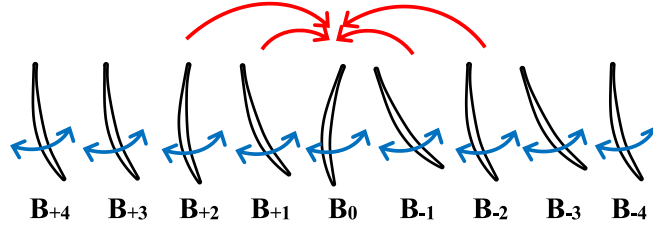


Fig. 4. Illustration of the source term superimposition method for the mistuned bladerow.

carried out in the training stage. Similarly to the classical ICM approach, only the middle blade is oscillated, while the adjacent blades are stationary. Fig. 3 shows the schematic illustration of the method with two adjacent blades retained on each side of the central blade. A five-blade configuration is usually deemed to be sufficient due to the convergence of influence as they travel away from the central blade. There are several evidences in the literature that the influence decays rapidly in the circumferential traveling direction (e.g. unsteady flow Phan and He, 2020, steady flow Lejon et al., 2020; Phan, 2022). The same finding holds even for mistuning cases (Lejon et al., 2020; Phan, 2022).

At each instantaneous central blade motion, the effects on itself and on the adjacent blades are recorded. The GISM truncated-domain fine mesh solution is projected onto the coarse mesh, thus enables the calculation of the source term $UST_{motion,m}$ for the blade passage m .

Then in the full-annulus configuration, each blade can vibrate in its own way according to the fluid–structure solution. The total source term applied to a reference passage $UST_{vibration}$ is a linear superposition of each individual passage's source term as in Eq. (17). Fig. 4 shows the schematic illustration of the source term superposition technique in the mistuned bladerow. In this example, only effects of the two closest adjacent blades on each side are shown, in accordance with the way the source term is calculated in the training stage.

Note that the GISM truncated-domain direct simulation in the training stage has a prescribed oscillation with known vibration amplitude and frequency. However, the fully-coupled solution would lead to vibration with a different amplitude (i.e. resonant against non-resonant) and frequency (i.e. frequency shift) at a different condition when the inlet distortion's frequency is swept through a potential range. To enable the application of the source term computed with the uncoupled GISM cascade to the fully-coupled solutions without repeating many training simulations, certain assumptions are made:

- (1) The source term coefficients are unchanged with vibration frequencies.
- (2) The source term coefficients scale linearly with the vibration amplitude.

The first assumption is valid because the frequency shift is typically small, thus the source term coefficients can be assumed to be constant with vibration frequency. The second assumption is justified because the response amplitudes are typically small enough to be within the linear range. For most experimental and numerical studies, the vibration amplitude is within the range 1% blade chord. For such vibration amplitude levels, the flow is pre-dominantly linear even with transonic flow conditions (Su et al., 2016; Bölcs and Fransson, 1986; Cinnela et al., 2004). It is imperative to realize that a new GISM cascade with the newly prescribed value of amplitude and frequency of interest can be recomputed to obtain more accurate source terms. However, these two above assumptions enable an efficient modeling method using a limited number of data available during the training phase.

5.4. Simulation setup

The current fully-coupled two-scale methodology is implemented in the commercial solver ANSYS CFX. The simulation domain comprises of 12 blade passages. The inlet boundary conditions include total pressure, total temperature, and flow angle. For the forced response calculation in the present work, a rotating inlet stagnation pressure distortion P_{01} with

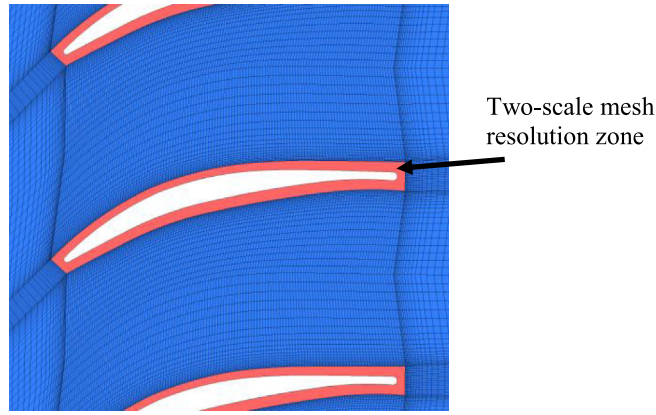


Fig. 5. Two-scale mesh resolution method applied to the boundary layer region.

known amplitude and frequency is imposed. The circumferential extent of one spatial period of inlet distortion covers 4 blade passages (i.e. a 12-passage domain has 3 periods of inlet distortion in the circumferential direction).

$$P_{01} = P_{01,uniform} + \Delta P_{01} \sin(\omega t + \theta_i) \quad (19)$$

where $P_{01,uniform}$ is the stagnation pressure at uniform inflow condition. ΔP_{01} is the distortion amplitude, which is taken to be equal to 10% of $P_{01,uniform}$. ω is the distortion rotating frequency and is swept near the blade natural frequency range to find its resonance response. θ_i is the relative phase angle between the i th and the first pitchwise grid line.

At the outlet, the static atmospheric pressure is used. The blades, hub, and casing surfaces are modeled as an adiabatic no-slip wall. The central idea of the two-scale method is around the use of two disparate mesh resolutions. In the current implementation, the boundary layer zone is chosen as the region of interest due to the typical requirement of sufficiently fine mesh to resolve the boundary layer on the blade surfaces. Fig. 5 highlights the application zone of the two-scale method. For the fine mesh computation, this boundary layer region is resolved for $y^+ < 1$. For the coarse and two-scale computations, this zone is coarsened in the wall normal direction (by a factor of 20). The under-resolved coarse mesh with a few elements in the boundary layer region would need to use the wall function model to approximate the near-wall region. The uncalibrated empirical wall function model could lead to erroneous results depending on the flow conditions as well as the surface regularities. It will be shown in the present work that the coarse mesh over-predicts the chordwise extension of mid-span bubble separation, which results in erroneous predictions of the unsteady flow characteristics.

Regarding the fully-coupled simulations, there are more than one way to initialize the blade motions. For self-excited vibrations, it has been shown that the non-traveling wave (single-blade) perturbation is more suitable for the mistuned calculation since it will excite all the possible modes (Phan and He, 2022b). On the other hand, for forced response problem, we will not initiate any blade perturbation but the motion is rather excited from rest by the inlet distortion. In addition, the blade mass ratio μ is another parameter of interest in fluid–structure interaction modeling:

$$\mu = \frac{m_{blade}}{\rho \pi (C/2)^2 h} \quad (20)$$

where m_{blade} is the blade mass, C is the blade chord, and h is the blade height.

The blade mass ratio represents the relative rigidity of the solid blade compared to the surrounding fluid. A representative value for solid turbomachinery blades is used with $\mu = 400$.

6. Validations

The representative geometry of modern compressor blading designs is adopted in the current work. This compressor blade geometry was among the first of its kind to be designed with an automatic optimization technique, followed by the work of Sanger (1983). Its tuned aerodynamic and aeroelastic performance were acquired from the oscillating cascade test (Yang and He, 2004). The experiment was conducted at a reduced Reynolds number, which encourages a bubble separation to form around mid-chord on the suction surface.

Table 1 shows a comparison between experimental and simulated operating conditions. Reynolds number Re and exit isentropic velocity V_{ref} are matched to a less than 5% discrepancy from the experimental conditions.

6.1. Steady flow

The laminar bubble separation was observed to form on the blade suction surface during the experiment. In the previous work (Phan and He, 2020), it was shown that using the two-equation $\gamma - \theta$ transition correlation coupled with the

Table 1
Experimental and numerical operating conditions.

Conditions	Experimental	Numerical
Re (based on blade chord and exit velocity) $\times 10^5$	1.95	1.967
Exit isentropic velocity V_{ref} , $m\ s^{-1}$	19.5	20.4

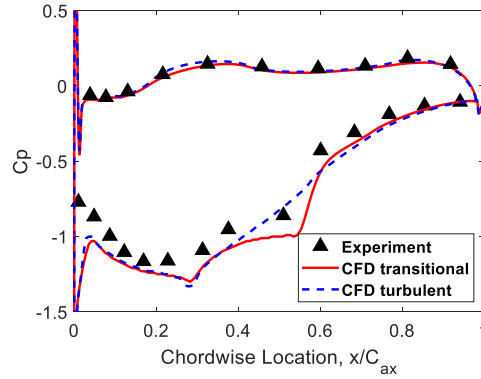


Fig. 6. Steady pressure distribution at mid-span.

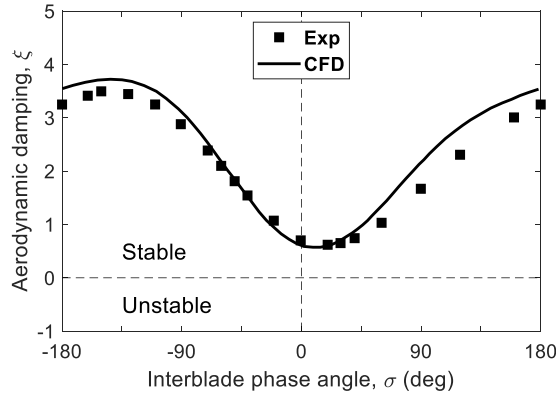


Fig. 7. Overall damping curve for bending mode at reduced frequency $k = 0.4$.

RANS SST model (Menter et al., 2006) is capable to predict the formation of separation bubble. On the other hand, the flow is smooth and no separation can be captured if the fully turbulent model is used. Fig. 6 presents the experimental steady pressure distribution at mid-span to that predicted by the direct fine mesh solution with transitional and turbulence models, confirming the previous findings. At mid-chord 40%C to 60%C, the transitional model can predict a plateau in the suction static pressure, which indicates the bubble formation. This is in agreement with the experimental data.

6.2. Steady flow

Next, the overall damping of the tuned oscillating cascade in the bending mode are validated against the experiment as shown in Fig. 7. In general, the computational results agree well with the experimental measurement across the whole range of IBPA. The most unstable inter-blade phase angle has been predicted fairly well at IBPA about 20 deg to 30 deg. For more extensive validation and analyses of the tuned oscillating cascade in the bending mode, particularly for the effects of laminar separation bubble and tip clearance on the aerodynamic damping, one is referred to Ref. Phan and He (2020).

7. Applications of the fully-coupled two-scale method

7.1. Case 1 – Tuned bladerow

The fully-coupled two-scale method is first applied to the classical tuned cascade, in which all blades have the same eigen-frequency, amplitude, and interblade phase angle. The distortion frequency is swept in the range close to the blade

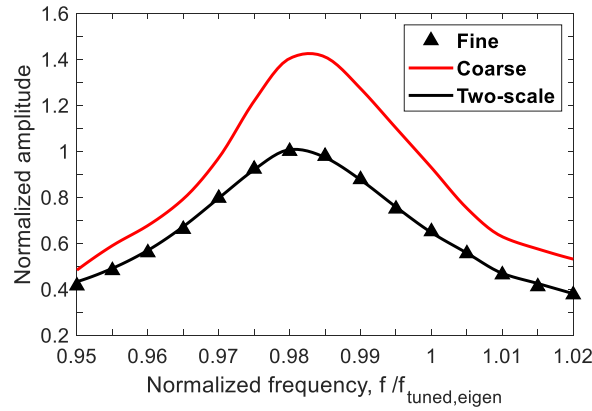


Fig. 8. Overall forced response curve of the tuned bladerow.

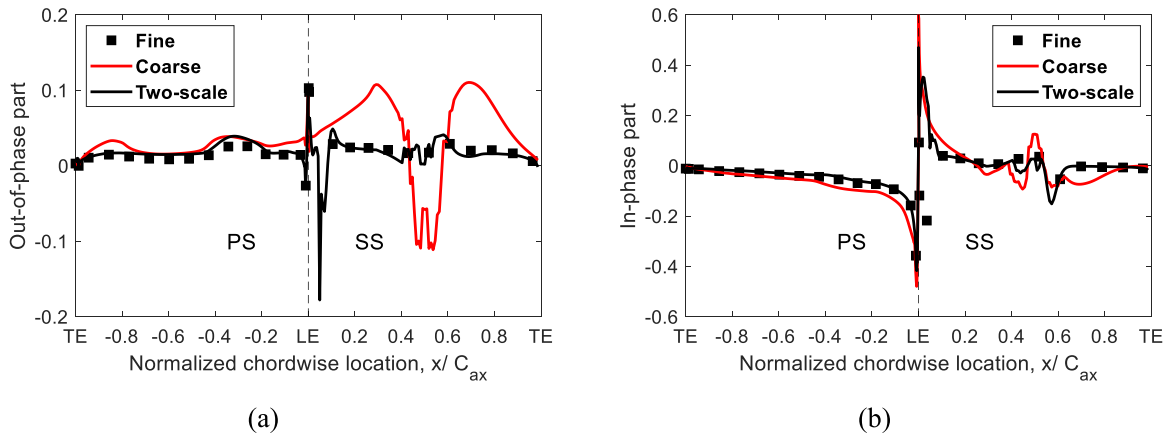


Fig. 9. 1st harmonic unsteady pressure responses on the blade surfaces of the tuned bladerow: (a) Out-of-phase component and (b) In-phase component.

eigen-frequency. Fig. 8 shows the overall forced response curve of the tuned cascade. The overall forced response curve has a bell shape, which indicates that the response amplitudes are higher near the resonance peak and getting smaller as moving away from the resonance. The x-axis in Fig. 8 represents the distortion frequency normalized to the eigen-frequency of the tuned cascade. It can be seen that the resonance peak does not take place at unity normalized frequency but at a slightly different frequency. This difference is known as the frequency shift, which is related to the fluid–structure coupling effects (Moffatt and He, 2005; Chahine et al., 2019). Regarding the prediction of forced response amplitude, the y-axis in Fig. 8 is normalized by the maximum amplitude predicted by the fine mesh simulation of the tuned cascade. The base coarse mesh simulation predicts a 50% higher amplitude response at the resonance peak compared to the fine mesh simulation. On the other hand, the newly developed two-scale method prediction is in good quantitative agreement with the fine mesh simulation for the whole forced response curve. The location and amplitude of the resonant peak are well-predicted by the fully-coupled two-scale method.

Fig. 9 shows the detailed unsteady pressure distribution on the blade surfaces at the resonance peak obtained by time-averaging the instantaneous data (see Ref. Phan (2021) for examples of such analysis method). Fig. 9a presents the out-of-phase component, while Fig. 9b presents the in-phase component of the 1st harmonic unsteady pressure. It is clear that the two-scale method predictions closely resemble that of the direct fine mesh simulation, whereas the coarse mesh predicts a qualitatively erroneous result in the mid-chord suction surface region. Thus, it can be said that the dynamic effects of the separation bubble can lead to over-prediction of the forced response amplitude.

7.2. Case 2 – Alternatingly mistuned bladerow

In this section, we start to investigate the mistuned bladerow, which is the main focus of the present work. In case 2, an alternating pattern of mistuning is used. This is the representative configuration of the intentional mistuning pattern for passive flutter alleviation (Corral et al., 2018). Fig. 10 shows the alternating mistuning pattern in comparison with its tuned counterpart. The mistuned eigen-frequency is within the range of $\pm 1\%$ deviated from that of tuned of bladerow.

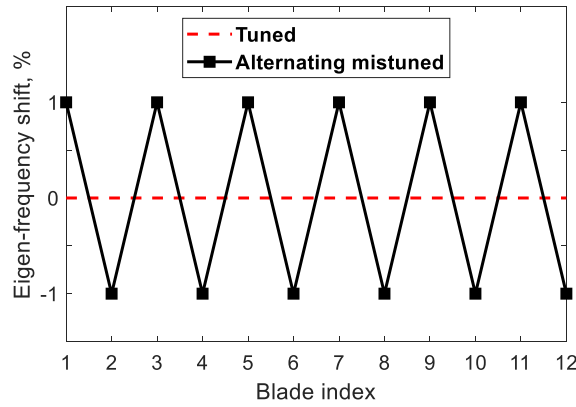


Fig. 10. Pattern of the alternating frequency mistuned bladerow.

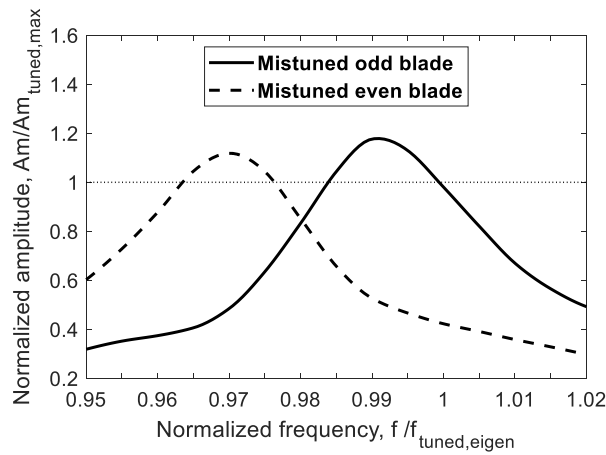


Fig. 11. Overall forced response curve of the alternating frequency mistuned bladerow.

First, we will explore what one would expect to observe in the forced response curve of the mistuned cascade. Fig. 11 shows the overall forced response curve of the alternating mistuned cascade. Since there are only two blade configurations of high and low eigen-frequency, we can clearly identify two separate curves corresponding to each blade. The first thing to note in Fig. 11 is the shift of resonance peaks. Odd-numbered blade has a higher eigen-frequency (see Fig. 11) and thus reaching a resonance peak at higher frequency compared to the tuned cascade (Figs. 11 vs. 8). A similar observation can be made for the even-numbered blade with lower eigen-frequency. Moreover, since the peak amplitude is of interest in the forced-response problems, we begin to turn our attention to the y-value of the curves. The mistuned response amplitude is normalized by the maximum tuned response amplitude. Therefore, a normalized amplitude higher than unity indicates an amplitude amplification factor, which represents the adverse effects of the mode localization phenomenon. The amplitude amplification can be seen around the peak responses of the mistuned blades, which reaches up to 20% higher than the tuned response for the current test case condition. Note that the amplification factor can be much higher depending on the mistuning level as well as the blade-to-blade coupling strength (Phan and He, 2022b).

Fig. 12 shows the comparisons of overall forced response curves predicted with different modeling fidelities. Fig. 12a is the set of curves corresponding the odd-numbered blade, while Fig. 12b represents that of the even-numbered blade. It can be seen that the fully-coupled two-scale method can significantly improve the response prediction compared to the base coarse mesh. The base coarse mesh predicts a fairly good response far away from the resonance peak. However, at vicinity of the resonance peak, the coarse mesh solution is highly erroneous with the response amplitude few times larger than that predicted by the fine mesh solution (up to 4 for the even-numbered blade).

Figs. 13 and 14 show the detailed unsteady pressure distribution on the blade surfaces at 97% normalized frequency for the odd-numbered and even-numbered blade, respectively. The results are time-averaged from the instantaneous data (Phan, 2021). This is the condition where the even-numbered blade reaches its resonance peak. It can be observed that the fully-coupled two-scale method can improve the local unsteady pressure distribution greatly for both cases. Unlike the case of tuned bladerow, this time the discrepancies exist all over the entire blade surfaces.

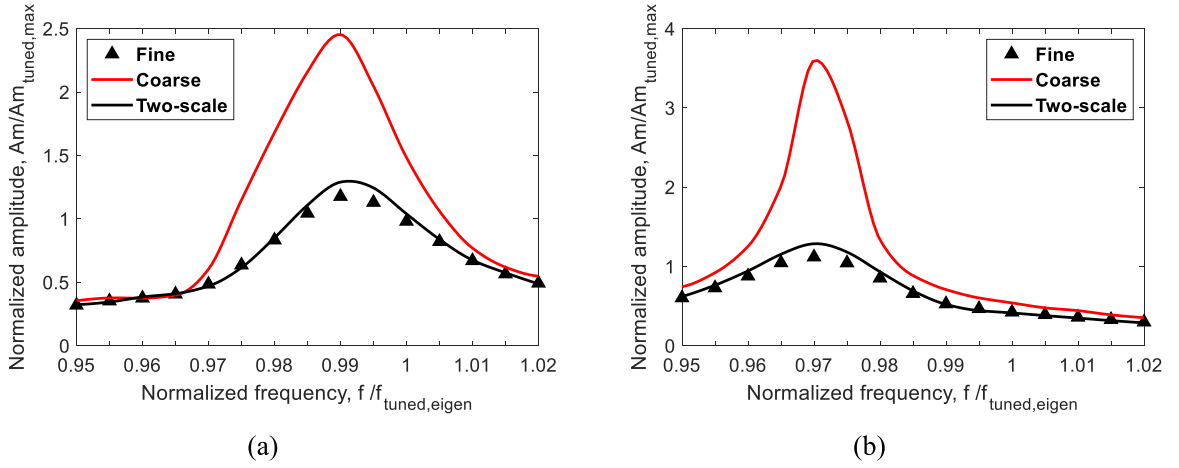


Fig. 12. Overall forced response curves of the alternating frequency mistuned bladerow predicted by different fidelities: (a) Odd-numbered blade and (b) Even-numbered blade.

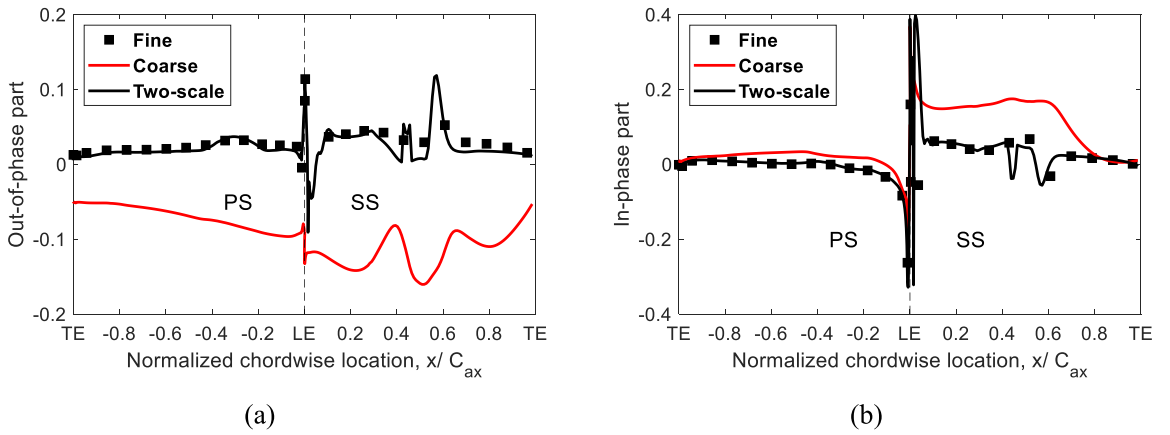


Fig. 13. 1st harmonic pressure responses on the odd-numbered blade surfaces of the alternating frequency mistuned bladerow: (a) Out-of-phase component and (b) In-phase component.

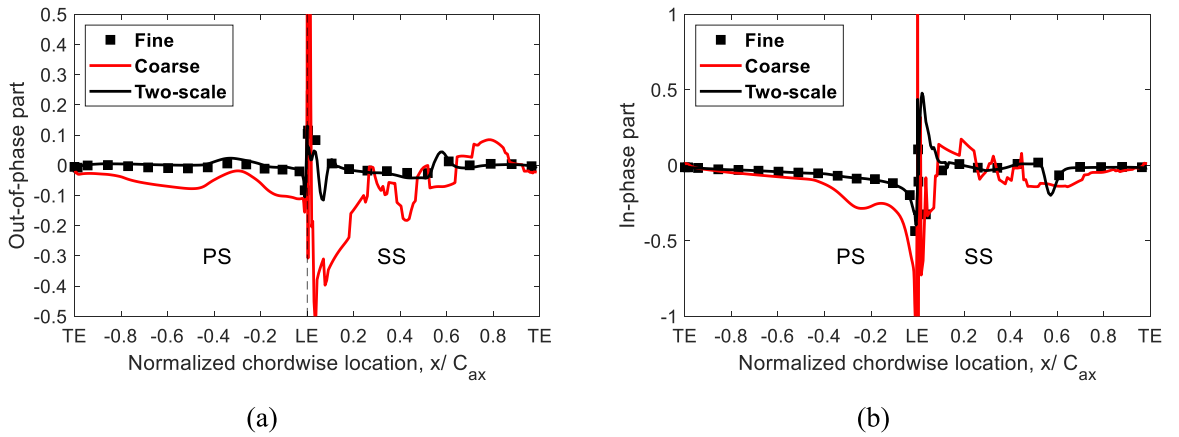


Fig. 14. 1st harmonic pressure responses on the even-numbered blade surfaces of the alternating frequency mistuned bladerow: (a) Out-of-phase component and (b) In-phase component.

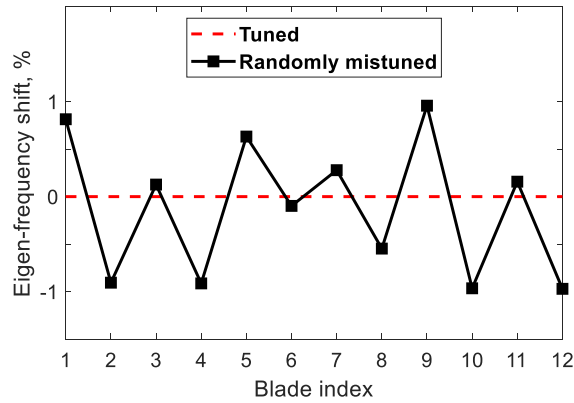


Fig. 15. Pattern of the random frequency mistuning case.

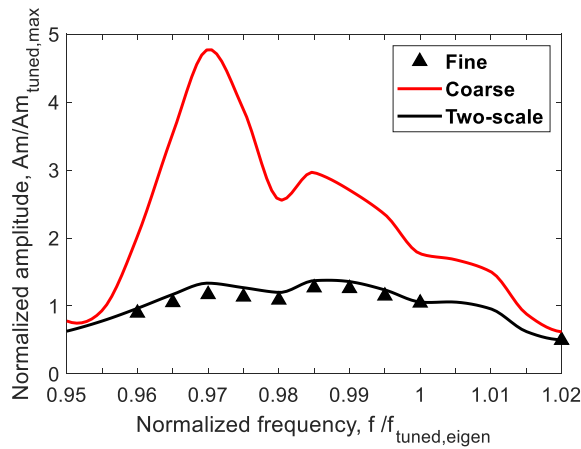


Fig. 16. Overall forced response curves of the random frequency mistuned bladerow predicted by different fidelities.

7.3. Case 3 — Randomly mistuned bladerow

Finally, we will apply the fully-coupled two-scale method on the randomly mistuned bladerow. This is a more realistic scenario because of the probabilistic nature of mistuning. Fig. 15 shows the pattern of the random frequency mistuning used in case 3. The randomly mistuned eigen-frequency is assumed to lie within the range of $\pm 1\%$ deviated from that of tuned of bladerow.

Fig. 16 shows the overall forced response curve of the randomly mistuned cascade bounded by the maximum amplitude at each respective frequency. The fully-coupled two-scale method is shown to improve the prediction accuracy significantly compared to the base coarse mesh. The coarse mesh predicts high vibration amplitudes up to 5 times different from what would be expected from the direct fine mesh solution. On the other hand, the two-scale method has a comparable accuracy to the fine mesh solution.

To further investigate the vibration kinematics of the random mistuning case, we shall look at each individual blade's dynamic as shown in Fig. 17. First thing to note is that the forced response level of the randomly mistuned bladerow is amplified up to the factor of 1.5 compared to the tuned bladerow. Secondly, the individual blade's response largely split into two main groups: one with higher eigen-frequencies and the other with lower eigen-frequencies compared to the tuned bladerow. The high-frequency group clusters on the right side of Fig. 17, while the low-frequency group clusters on the left side. This is in agreement with the observation in the alternately mistuned case, where the frequency mistuning scatters the blade responses according to their eigen-frequencies. It can also be seen that most of the blades have higher amplitude responses than the tuned blade.

Fig. 18 shows the detailed unsteady pressure distribution on the blade surfaces at the resonance peak. The results are time-averaged from the instantaneous data (Phan, 2021). Fig. 18a presents the out-of-phase component, while Fig. 18b presents the in-phase component of the 1st harmonic unsteady pressure. Apparently the two-scale method predictions are in good agreement with the direct fine mesh simulation. On the other hand, the coarse mesh simulation predicts a

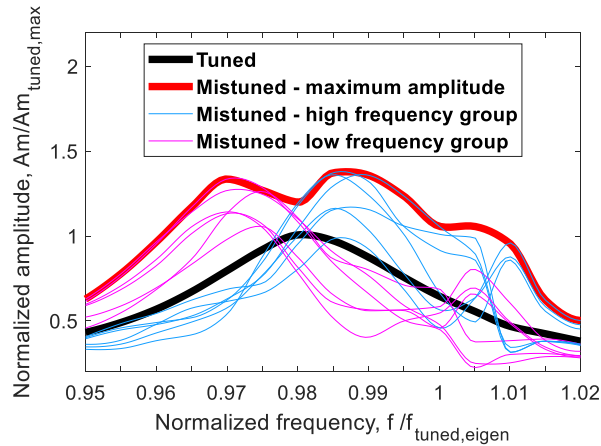


Fig. 17. Overall forced response curves of the random frequency mistuned bladerow. (For interpretation of the references to color in this figure legend, the reader is referred to the web version of this article.)

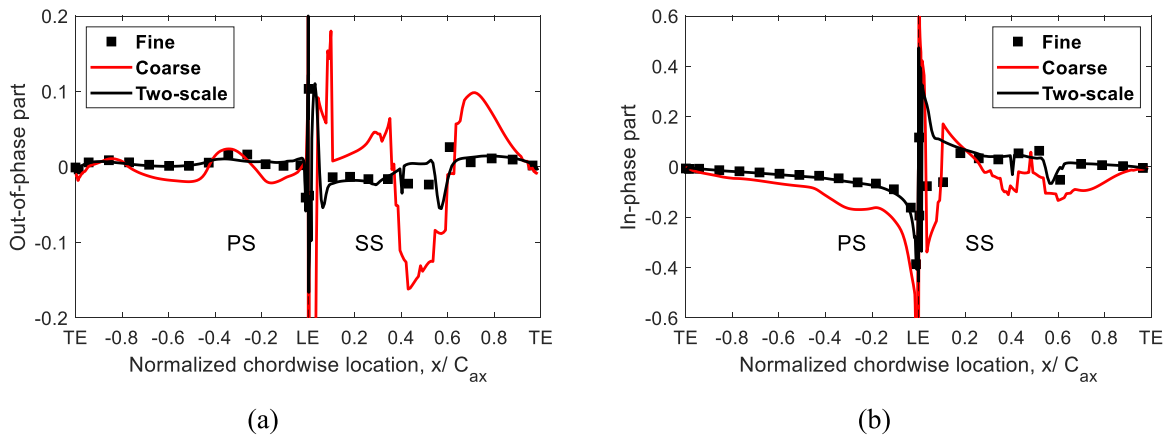


Fig. 18. 1st harmonic pressure responses on the maximum amplitude blade surfaces of the randomly frequency mistuned bladerow: (a) Out-of-phase component and (b) In-phase component.

substantially different result, particularly on the blade suction surface. These local differences add up to produce a much larger amplitude response in the coarse mesh.

Fig. 19 compares the instantaneous entropy function contour predicted by different modeling fidelities. Three high entropy peaks and troughs can be observed passing through the bladerow, in agreement with the imposed inlet distortion pattern. Although the overall entropy distribution of the direct coarse mesh simulation looks qualitatively similar to that of the fine mesh, we pay attention to some notable discrepancies. Firstly, the wakes predicted by the coarse mesh are significantly thicker than that of the direct fine mesh. Note that the mesh resolution in the wake regions are the same for all modeling configurations. The disparate mesh resolution is only applied to the boundary layer zone (see **Fig. 5**). Thus, it can be deduced that the near-wall coarsen boundary layer region does not only deteriorate the blade loading but also propagate errors downstream, further into the wake mixing region. This observation somewhat agrees with the previous finding using the uncoupled method, in which the coarse mesh's static pressure errors were seen to propagate both upstream and downstream of the bladerow (**Phan and He, 2021**). For this particular test case and condition, this discrepancy stems from the over-prediction of the bubble separation size in the coarse mesh simulation, thus creating a large low-momentum region on the blade suction surface that leaves the trailing edge and thickens the wake. Secondly, the coarse mesh simulation predicts an asymmetric wake mixing pattern, highlighted inside the dashed circle near the bladerow exit. This asymmetric distribution is produced by the interaction between the passing entropy waves and the blade wakes (thus also the blade vibrations). Remarkably, both two aforementioned discrepancies between the fine and coarse mesh simulations do not exist for the fully-coupled two-scale method. This finding suggests that the new method has corrected the error in the base coarse mesh computation. Moreover, the interactions between the inlet distortion and the blade vibration can be reproduced by the two-scale method despite of its uncoupled approach to determine separately the source term attributed to each flow disturbance.

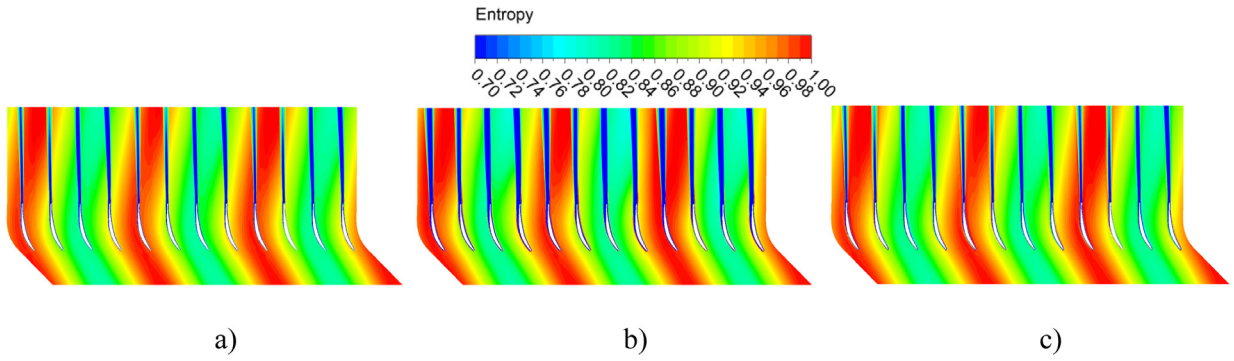


Fig. 19. Instantaneous entropy function $e^{(-\Delta s/R)}$ contour of different modeling fidelities for the randomly mistuned bladerow: (a) Direct fine mesh, (b) Direct coarse mesh, and (c) Fully-coupled two-scale. (For interpretation of the references to color in this figure legend, the reader is referred to the web version of this article.)

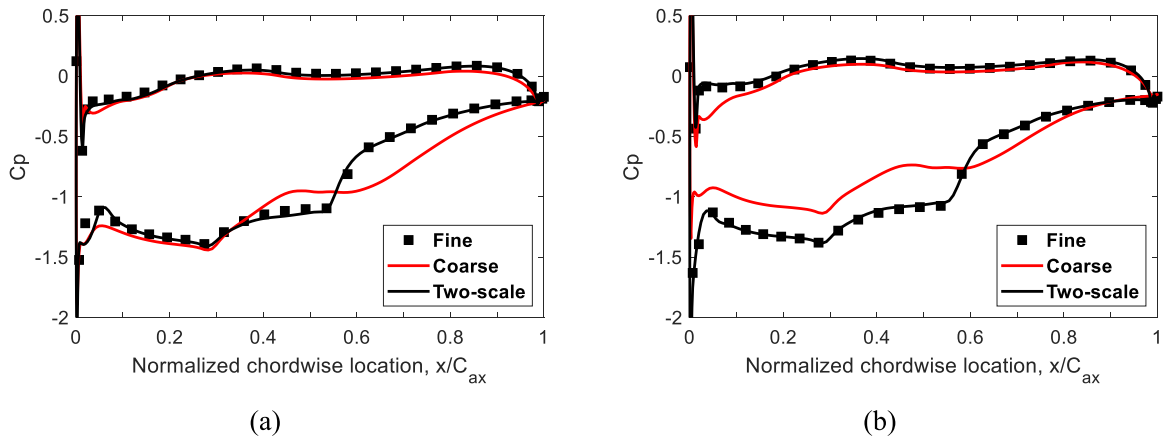


Fig. 20. Instantaneous blade static pressure distribution for the forced response of the randomly mistuned bladerow: (a) Blade 2 — minimum entropy wake and (b) Blade 4 — maximum entropy wake.

Fig. 20 shows the comparison of the instantaneous static pressure distribution for different blades. Fig. 20a presents the results for the blade subject to the minimum entropy wake (trough), while Fig. 20b shows that for the blade immersed in the maximum entropy wake (peak). For both blades, the two-scale method can be seen to be in excellent agreement with the direct fine mesh solution. The coarse mesh solution for Blade 2 over-predicts the size of bubble separation. On the other hand, the blade loading of Blade 4 significantly under-predicted by the coarse mesh simulation.

Fig. 21 shows the instantaneous wake traverse at $x/C_{ax} = 1.7$. The peak entropy loss in the wake region is over-predicted by the coarse mesh simulation, while the fully-coupled two-scale method are in excellent agreement with the fine mesh solution. This result supports the analysis of the wake mixing in the above discussion. This finding suggests that the fully-coupled two-scale method is not only useful for aeroelastic but also for aerodynamic analyses, where the entropy loss is of interest to understand the loss mechanism (Denton, 1993).

8. Conclusions

In this paper, an efficient method is introduced to predict the aeroelastic performance of a mistuned bladerow using the fully-coupled method. The two-scale approach is embedded in the fully-coupled procedure, resulting in an efficient and accurate methodology. The validity and effectiveness of the method is examined through the case studies for a forced response bladerow. The new method has the following features:

- (1) Only a single unsteady forcing simulation with stationary blades and a single GISM truncated-domain simulation (with only one blade vibrating) for a tuned bladerow, are required to generate the source terms.
- (2) The whole forced response characteristics for different frequencies, amplitudes, and mistuning patterns can then be simulated efficiently with the superimposed source terms.
- (3) The fluid–structure interaction effects are taken into account by the fully-coupled method.

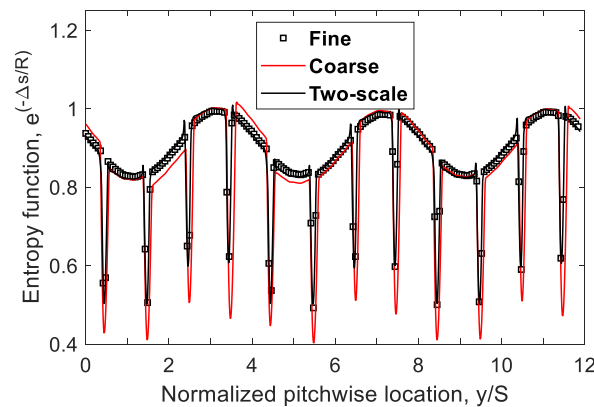


Fig. 21. Overall forced response curves of the random frequency mistuned bladerow.

The proposed method has been validated against the direct fully coupled fine mesh solutions in test cases including tuned, alternately mistuned, and randomly mistuned bladerows. It is shown that the present fully-coupled two-scale method has a good accuracy both qualitatively and quantitatively compared to the direct baseline fine-mesh solutions, while being up to one order of magnitude faster. Although the pre-computed source terms are sampled at a particular frequency and amplitude, the procedure is shown to work effectively for a range of frequencies and amplitudes encountered during the frequency sweeping process. In addition, the new method is also shown to be able to capture the interactions between the inlet distortion and the blade vibration, although the source terms are determined in an uncoupled manner.

The forced response behavior predicted by the present fully coupled approach shows the frequency-shift from the eigenfrequency at resonance depends on the amount of frequency mistuning. In addition, the alternating and random mistuning patterns examined in the present work are shown to amplify the forced response levels up to 20% and 50% respectively compared to that of a baseline tuned bladerow.

After assessing the accuracy of the fully-coupled two-scale method, we turn our attention to its computational efficiency. It can be seen easily that the efficiency of the proposed method depends on the mesh reduction factor between the fine mesh and the coarse mesh. In the present examples used in this paper, we are able to achieve a reduction in computational time up to 7 times faster compared to the baseline case of fine mesh. The computational reduction factor is roughly equal to the *global* mesh reduction factor. Note that in the present two-dimensional example we only coarsen the mesh in the *local* boundary layer region (with reduction factor of 20). One is able to achieve a more significant reduction in computational time if the mesh is coarsened in the global blade passage domain as well as extending to the three-dimensional mesh coarsening.

The results demonstrated in the present work has proved its potential to increase the numerical prediction efficiency for a mistuned bladerow's aeroelastic assessment. However, future works will need to be carried out to validate the new method for a range of challenging conditions. For example, the value of blade mass ratio μ can be further reduced significantly to the representative level of a composite structure. The blade structure will be more flexible and the accuracy of the GISM assumptions shall be assessed. In addition, the range of mistuning magnitude should also be validated. For small values of mistuning magnitude typical to that of manufacturing variations, the GISM has been shown to be valid in the present work as well as in the literature. For a large value of mistuning magnitude (e.g. intentional mistuning), the method needs to be assessed in terms of accuracy.

CRedit authorship contribution statement

H.M. Phan: Conceptualization, Methodology, Software, Validation, Formal analysis, Investigation, Writing – original draft, Writing – review & editing, Visualization. **L. He:** Conceptualization, Methodology, Formal analysis, Investigation, Writing – original draft, Writing – review & editing.

Declaration of competing interest

The authors declare that they have no known competing financial interests or personal relationships that could have appeared to influence the work reported in this paper.

Data availability

Data will be made available on request.

Acknowledgments

The support from the EPSRC, United Kingdom CDT in Gas Turbine Aerodynamics is much appreciated. The work is partly sponsored by the Chair of Computational Aerothermal Engineering Bursary, United Kingdom. The author would like to acknowledge the use of the University of Oxford Advanced Research Computing (ARC) facility in carrying out this work (<https://doi.org/10.5281/zenodo.22558>).

References

- Bölcs, A., Fransson, T.H., 1986. Aeroelasticity in Turbomachines: Comparison of Theoretical and Experimental Cascade Results. Communication (13) Lab de Thermique Appliquee, Ecole Polytechnique Federale de Lausanne (EPFL), Switzerland.
- Chahine, C., Verstraete, T., He, L., 2019. A comparative study of coupled and decoupled fan flutter prediction methods under variation of mass ratio and blade stiffness. *J. Fluids Struct.* 85, 110–125.
- Chen, T., Vasanthakumar, P., He, L., 2001. Analysis of unsteady bladerow interaction using nonlinear harmonic approach. *J. Propuls. Power* 17 (3), 651–658.
- Chiang, H.D., Kielb, R.E., 1993. An analysis system for blade forced response. *J. Turbomach.* 115 (4), 762–770.
- Cinnela, P., De Palma, P., Pascasio, G., Napolitano, M., 2004. A numerical method for turbomachinery aeroelasticity. *J. Turbomach.* 126 (2), 310–316.
- Corral, R., Khemiri, O., Martel, C., 2018. Design of mistuning patterns to control the vibration amplitude of unstable rotor blades. *Aerosp. Sci. Technol.* 80, 20–28.
- Denton, J.D., 1993. The 1993 IGTI scholar lecture: Loss mechanisms in turbomachines. *J. Turbomach.* 115 (4), 621–656.
- Giles, M.B., 1990. Stator/rotor interaction in a transonic turbine. *J. Propuls. Power* 6 (5), 621–627.
- Hall, K.C., Ekici, K., 2005. Multistage coupling for unsteady flows in turbomachinery. *AIAA J.* 43 (3), 624–632.
- Hall, K.C., Thomas, J.P., Clark, W.S., 2002. Computation of unsteady nonlinear flows in cascades using a harmonic balance technique. *AIAA J.* 40 (5), 879–886.
- Hanamura, Y., Tanaka, H., Yamaguchi, K., 1980. A simplified method to measure unsteady forces acting on the vibrating blades in cascade. *Bull. JSME* 23 (180), 880–887.
- He, L., 2010. Fourier methods for turbomachinery applications. *Prog. Aerosp. Sci.* 46 (8), 329–341.
- He, L., 2013. Block-spectral mapping for multi-scale solution. *J. Comput. Phys.* 250, 13–26.
- He, L., 2018. Multiscale block spectral solution for unsteady flows. *Internat. J. Numer. Methods Fluids* 86 (10), 655–678.
- He, Z., Epureanu, B.I., Pierre, C., 2007. Fluid-structural coupling effects on the dynamics of mistuned bladed disks. *AIAA J.* 45 (3), 552–561.
- He, L., Ning, W., 1998. Efficient approach for analysis of unsteady viscous flows in turbomachines. *AIAA J.* 36 (11), 2005–2012.
- Kelly, S.T., Lupini, A., Epureanu, B.I., 2021. Data-driven modeling approach for mistuned cyclic structures. *AIAA J.* 59 (7), 2684–2696.
- Lejon, M., Andersson, N., Ellbrant, L., Mårtensson, H., 2020. The impact of manufacturing variations on performance of a transonic axial compressor rotor. *J. Turbomach.* 142 (8), 081009.
- Leng, Y., Key, N.L., 2020. Effects of nonuniform blade spacing on compressor rotor forced response and aeroacoustics. *J. Propuls. Power* 20 (1), 108–188.
- Martel, C., Sánchez-Álvarez, J.J., 2017. Maximum mistuning amplification of the forced response vibration of turbomachinery rotors in the presence of aerodynamic damping. *J. Sound Vib.* 397, 108–122.
- Menter, F.R., Langtry, R.B., Likki, S.R., Suzen, Y.B., Huang, P.G., Völker, S., 2006. A correlation-based transition model using local variables – Part I: Model formulation. *J. Turbomach.* 128 (3), 413–422.
- Miyakozawa, T., Kielb, R.E., Hall, K.C., 2009. The effects of aerodynamic perturbations on forced response of bladed disks. *J. Turbomach.* 131 (4), 041008.
- Moffatt, S., He, L., 2005. On decoupled and fully-coupled methods for blade forced response prediction. *J. Fluids Struct.* 20 (2), 217–234.
- Moffatt, S., Ning, W., Li, Y., Wells, R.G., He, L., 2005. Blade forced response prediction for industrial gas turbines. *J. Propuls. Power* 21 (4), 707–714.
- Ning, W.E.I., He, L., 2001. Some modeling issues on trailing-edge vortex shedding. *AIAA J.* 39 (5), 787–793.
- Petrov, E.P., 2010. A method for forced response analysis of mistuned bladed disks with aerodynamic effects included. *J. Eng. Gas Turbines Power* 132 (6), 062502.
- Phan, H.M., 2021. A spatial-temporal analysis approach for flutter predictions using decoupled and fully-coupled methods. *J. Fluids Struct.* 107, 103412.
- Phan, H.M., 2022. Modeling of a turbine bladerow with stagger angle variation using the multi-fidelity influence superposition method. *Aerosp. Sci. Technol.* 121, 107318.
- Phan, H.M., He, L., 2020. Validation studies of linear oscillating compressor cascade and use of influence coefficient method. *J. Turbomach.* 142 (5), 051005.
- Phan, H.M., He, L., 2021. Efficient steady and unsteady flow modeling for arbitrarily mis-staggered bladerow under influence of inlet distortion. *J. Eng. Gas Turbines Power* 143 (7), 071009.
- Phan, H.M., He, L., 2022a. Phasing Structural and Aerodynamic Mistuning for Leveraging Aeroelastic Performance. *ASME Paper No. GT2022-82168*.
- Phan, H.M., He, L., 2022b. Investigation of structurally and aerodynamically mistuned oscillating cascade using fully coupled method. *J. Eng. Gas Turbines Power* 144 (3), 031009.
- Sadeghi, M., Liu, F., 2005. Computation of cascade flutter by uncoupled and coupled methods. *Int. J. Comput. Fluid Dyn.* 19 (8), 559–569.
- Sanger, N.L., 1983. The use of optimization techniques to design-controlled diffusion compressor blading. *J. Eng. Gas Turbines Power* 105 (2), 256–264.
- Sicot, F., Dufour, G., Gourdain, N., 2012. A time-domain harmonic balance method for rotor/stator interactions. *J. Turbomach.* 134 (1), 011001.
- Sicot, F., Gomar, A., Dufour, G., Dugeai, A., 2014. Time-domain harmonic balance method for turbomachinery aeroelasticity. *AIAA J.* 52 (1), 62–71.
- Su, D., Zhang, W., Ye, Z., 2016. A reduced order model for uncoupled and coupled cascade flutter analysis. *J. Fluids Struct.* 61, 410–430.
- Tran, D.M., 2009. Multi-parameter aerodynamic modeling for aeroelastic coupling in turbomachinery. *J. Fluids Struct.* 25 (3), 519–534.
- Yang, H., He, L., 2004. Experimental study on linear compressor cascade with three-dimensional blade oscillation. *J. Propuls. Power* 20 (1), 108–188.